Article

Self-Assembly of Supramolecular Light-Harvesting Arrays from Covalent Multi-Chromophore Perylene-3,4:9,10-bis(dicarboximide) Building Blocks

Michael J. Ahrens, Louise E. Sinks, Boris Rybtchinski, Wenhao Liu, Brooks A. Jones, Jovan M. Giaimo, Alexy V. Gusev, Andrew J. Goshe, David M. Tiede, and Michael R. Wasielewski

J. Am. Chem. Soc., **2004**, 126 (26), 8284-8294• DOI: 10.1021/ja039820c • Publication Date (Web): 05 June 2004

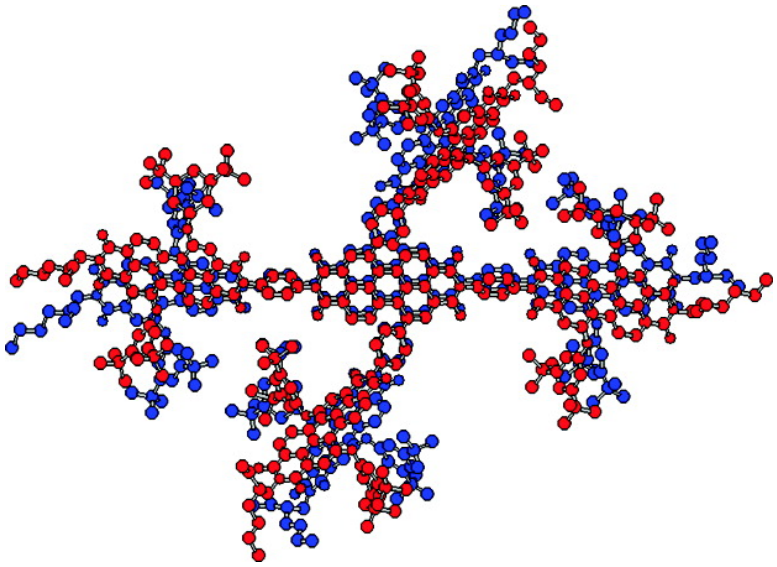

J|A|C|S
ARTICLES
Published on Web 06/05/2004

Self-Assembly of Supramolecular Light-Harvesting Arrays from Covalent Multi-Chromophore Perylene-3,4:9,10-bis(dicarboximide) Building Blocks

Michael J. Ahrens,[†] Louise E. Sinks,[†] Boris Rybtchinski,[†] Wenhao Liu,[†] Brooks A. Jones,[†] Jovan M. Giaimo,[†] Alexy V. Gusev,[†] Andrew J. Goshe,[‡] David M. Tiede,[‡] and Michael R. Wasielewski*,[†]

Contribution from the Department of Chemistry and Center for Nanofabrication and Molecular Self-Assembly, Northwestern University, Evanston, Illinois 60208-3113, and Chemistry Division, Argonne National Laboratory, Argonne, Illinois 60439

Received November 26, 2003; E-mail: wasielew@chem.northwestern.edu

Abstract: We report on two multi-chromophore building blocks that self-assemble in solution and on surfaces into supramolecular light-harvesting arrays. Each building block is based on perylene-3,4:9,10-bis(dicarboximide) (PDI) chromophores. In one building block, *N*-phenyl PDI chromophores are attached at their para positions to both nitrogens and the 3 and 6 carbons of pyromellitimide to form a cross-shaped molecule ($PI\text{-}PDI_4$). In the second building block, *N*-phenyl PDI chromophores are attached at their para positions to both nitrogens and the 1 and 7 carbons of a fifth PDI to produce a saddle-shaped molecule (PDI_5). These molecules self-assemble into partially ordered dimeric structures $(PI\text{-}PDI_4)_2$ and $(PDI_5)_2$ in toluene and 2-methyltetrahydrofuran solutions with the PDI molecules approximately parallel to one another primarily due to $\pi-\pi$ interactions between adjacent PDI chromophores. On hydrophobic surfaces, PDI_5 grows into rod-shaped nanostructures of average length 130 nm as revealed by atomic force microscopy. Photoexcitation of these supramolecular dimers in solution gives direct evidence of strong $\pi-\pi$ interactions between the excited PDI chromophore and other PDI molecules nearby based on the observed formation of an excimer-like state in $<$130 fs with a lifetime of about 20 ns. Multiple photoexcitations of the supramolecular dimers lead to fast singlet−singlet annihilation of the excimer-like state, which occurs with exciton hopping times of about 5 ps, which are comparable to those observed in photosynthetic light-harvesting proteins from green plants.

Introduction

The preparation of molecular photonic devices such as solar cells, light-emitting diodes, organic electronic components, and sensors frequently requires the assembly of well-ordered materials in which energy and charge transport are rapid and directional.[1−7] For many years photosynthetic antenna and reaction center proteins have served as important models for designing chemical systems optimized for energy and electron transport.[1,2] An important feature of these proteins that differs from most model systems is the fact that none of their energy or electron transport chromophores are covalently linked to one another. The protein structure provides specific distances and orientations between the chromophores as well as an electronic environment that is critical to proper functioning of the system. Over the past few years we have developed several approaches to controlling charge transport in organic nanostructures that take advantage of the speed and efficiency of ultrafast photoinduced electron-transfer reactions.[8−11] However, as the size and complexity of these systems have grown, it has become apparent that a new strategy based on a combination of synthetic covalent building blocks and self-assembly has significant advantages for producing photofunctional materials. We are currently exploring an approach using functional covalent building blocks having structures designed to elicit particular self-assembly motifs to produce supramolecular photofunctional materials. In this way, we can optimize their energy and charge transport properties without resynthesizing the complete system. This approach also offers the possibility that materials can be made

[†] Northwestern University.
[‡] Argonne National Laboratory.

(1) Wasielewski, M. R. *Chem. Rev.* **1992**, *92*, 435−461.
(2) Gust, D.; Moore, T. A.; Moore, A. L. *Acc. Chem. Res.* **2001**, *34*, 40−48.
(3) Wagner, R. W.; Lindsey, J. S.; Seth, J.; Palaniappan, V.; Bocian, D. F. *J. Am. Chem. Soc.* **1996**, *118*, 3996−3997.
(4) Würthner, F.; Thalacker, C.; Diele, S.; Tschierske, C. *Chem.—Eur. J.* **2001**, *7*, 2245−2253.
(5) Aratani, N.; Osuka, A.; Cho, H. S.; Kim, D. *J. Photochem. Photobiol., C.* **2002**, *3*, 25−52.
(6) Jordens, S.; De Belder, G.; Lor, M.; Schweitzer, G.; Van der Auweraer, M.; Weil, T.; Herrmann, A.; Wiesler, U.-M.; Müllen, K.; De Schryver, F. C. *Photochem. Photobiol. Sci.* **2003**, *2*, 1118−1124.
(7) Furuta, P.; Brooks, J.; Thompson, M. E.; Frechet, J. M. J. *J. Am. Chem. Soc.* **2003**, *125*, 13165−13172.
(8) Gosztola, D.; Niemczyk, M. P.; Wasielewski, M. R. *J. Am. Chem. Soc.* **1998**, *120*, 5118−5119.
(9) Hayes, R. T.; Wasielewski, M. R.; Gosztola, D. *J. Am. Chem. Soc.* **2000**, *122*, 5563−5567.
(10) Lukas, A. S.; Bushard, P. J.; Wasielewski, M. R. *J. Am. Chem. Soc.* **2001**, *123*, 2440−2441.
(11) Andersson, M.; Sinks, L. E.; Hayes, R. T.; Zhao, Y.; Wasielewski, M. R. *Angew. Chem., Int. Ed.* **2003**, *42*, 3139−3143.

10.1021/ja039820c CCC: $27.50

in which defects can be removed by disassembly-assembly cycles.

Covalent syntheses of large, ordered molecular arrays are usually inefficient and costly, thus making self-assembly the method of choice to achieve ordered architectures from functional building blocks. Self-assembly can be based on a variety of weak interactions such as hydrogen bonding[12−16] or $\pi-\pi$ interactions.[17−19] We recently reported on a photofunctional self-assembled array consisting of a zinc *meso*-tetraphenylporphyrin (ZnTPP) with four perylene-3,4:9,10-bis(dicarboximide) (PDI) chromophores covalently attached to the para positions of the phenyl groups (ZnTPP−PDI_4).[20] This covalent antenna/reaction center molecule self-assembles into supramolecular structures having significant order among the ZnTPP−PDI_4 building blocks. Photoinduced electron transfer from the ZnTPP to one of its attached PDI acceptors occurs in 3 ps and is followed by electron transport among several neighboring noncovalently attached PDI molecules within the assembly. The ability to photogenerate charges with nearly 100% quantum yield and have the resultant charges readily migrate within a material is important for its potential utilization in solar cell applications.

Another desirable characteristic of chromophore arrays for use in solar cells is efficient energy transport. Good multi-chromophore antenna arrays not only have excellent cross sections for light absorption but also in addition carry out internal energy transport rapidly and efficiently to deliver singlet excitons to sites at which charge separation can occur. Antenna proteins in photosynthetic organisms fulfill these requirements using many chlorophyll molecules to transport singlet excitons to the primary electron donor chlorophyll within a nearby reaction center protein leading to charge separation in a few picoseconds.[21] Several elegant multi-porphyrin covalent arrays have been prepared and used to study energy transport.[5,22−30] Recent examples involving both planar and linear porphyrin arrays show that the electronic properties of the covalent linkages between the porphyrins and the electronic structure of the two nearly degenerate highest occupied molecular orbitals of the porphyrin play important roles in determining rates of energy transfer.[27] Dendrimeric systems having many aromatic molecules, such as polyphenylbenzenes and perylene-3,4-dicarboximides, have been used to elucidate the details of energy transport within complex covalent structures as well as the photophysics of single molecules having multiple chromophores.[6,7,31−37] Thus far, studies of energy transport in arrays consisting of many chromophores have been focused largely on polymers,[38−45] self-assembled structures made from single chromophores[4,46−48] and dendrimeric metal complexes.[49−51] We now report on two antenna arrays based on PDI, a chromophore that has been well characterized previously along with other closely related derivatives.[47,48,52−58] Unlike our earlier work with $(ZnTPP-PDI_4)_n$ arrays, which was focused on efficient *electron* transfer, the new systems presented here are designed to explore molecular architectures to create an efficient *energy* transport material. These covalent multi-chromophore arrays, PI-PDI_4 and PDI_5, Figure 1, self-assemble into partially ordered photofunctional supramolecular structures using $\pi-\pi$ interactions among the PDI chromophores. Photophysical studies show that energy transport within these supramolecular antenna structures is both rapid and efficient.

(12) Kotera, M.; Lehn, J.-M.; Vigneron, J.-P. *Tetrahedron* **1995**, *51*, 1953−1972.
(13) Sessler, J. L.; Wang, B.; Harriman, A. *J. Am. Chem. Soc.* **1995**, *117*, 704−714.
(14) Springs, S. L.; Andrievsky, A.; Kral, V.; Sessler, J. L. *J. Porphyrins Phthalocyanines* **1998**, *2*, 315−325.
(15) Arimura, T.; Ide, S.; Sugihara, H.; Murata, S.; Sessler, J. L. *New J. Chem.* **1999**, *23*, 977−979.
(16) Berg, A.; Shuali, Z.; Asano-Someda, M.; Levanon, H.; Fuhs, M.; Möbius, K.; Wang, R.; Brown, C.; Sessler, J. L. *J. Am. Chem. Soc.* **1999**, *121*, 7433−7434.
(17) Hunter, C. A.; Sanders, J. K. M. *J. Am. Chem. Soc.* **1990**, *112*, 5525−5534.
(18) Shimomura, M.; Olaf, K.; Ijiro, K. *Synth. Met.* **1996**, *81*, 251−257.
(19) Zangmeister, R. A. P.; Smolenyak, P. E.; Drager, A. S.; O'Brien, D. F.; Armstrong, N. R. *Langmuir* **2001**, *17*, 7071−7078.
(20) van der Boom, T.; Hayes, R. T.; Zhao, Y.; Bushard, P. J.; Weiss, E. A.; Wasielewski, M. R. *J. Am. Chem. Soc.* **2002**, *124*, 9582−9590.
(21) Diner, B. A.; Babcock, G. T. *Adv. Photosynth.* **1996**, 4, 213−247.
(22) Ikonen, M.; Guez, D.; Marvaud, V.; Markovitsi, D. *Chem. Phys. Lett.* **1994**, *231*, 93−97.
(23) Wagner, R. W.; Johnson, T. E.; Lindsey, J. S. *J. Am. Chem. Soc.* **1996**, *118*, 11166−11180.
(24) Seth, J.; Palaniappan, V.; Wagner, R. W.; Johnson, T. E.; Lindsey, J. S.; Bocian, D. F. *J. Am. Chem. Soc.* **1996**, *118*, 11194−11207.
(25) Hsiao, J.-S.; Krueger, B. P.; Wagner, R. W.; Johnson, T. E.; Delaney, J. K.; Mauzerall, D. C.; Fleming, G. R.; Lindsey, J. S.; Bocian, D. F.; Donohoe, R. J. *J. Am. Chem. Soc.* **1996**, *118*, 11181−11193.
(26) Strachan, J.-P.; Gentemann, S.; Seth, J.; Kalsbeck, W. A.; Lindsey, J. S.; Holten, D.; Bocian, D. F. *J. Am. Chem. Soc.* **1997**, *119*, 11191−11201.
(27) Yang, S. I.; Seth, J.; Balasubramanian, T.; Kim, D.; Lindsey, J. S.; Holten, D.; Bocian, D. F. *J. Am. Chem. Soc.* **1999**, *121*, 4008−4018.
(28) Tsuda, A.; Osuka, A. *Science (Washington, DC, United States)* **2001**, *293*, 79−82.
(29) Tsuda, A.; Osuka, A. *J. Inclusion Phenom. Macrocyclic Chem.* **2001**, *41*, 77−81.
(30) Tsuda, A.; Osuka, A. *Adv. Mater. (Weinheim, Germany)* **2002**, *14*, 75−79.
(31) Cotlet, M.; Gronheid, R.; Habuchi, S.; Stefan, A.; Barbafina, A.; Müllen, K.; Hofkens, J.; De Schryver, F. C. *J. Am. Chem. Soc.* **2003**, *125*, 13609−13617.
(32) Hofkens, J.; Maus, M.; Gensch, T.; Vosch, T.; Cotlet, M.; Koehn, F.; Herrmann, A.; Müllen, K.; De Schryver, F. *J. Am. Chem. Soc.* **2000**, *122*, 9278−9288.
(33) Vosch, T.; Cotlet, M.; Hofkens, J.; Van Biest, K.; Lor, M.; Weston, K.; Tinnefeld, P.; Sauer, M.; Latterini, L.; Müllen, K.; De Schryver, F. C. *J. Phys. Chem. A* **2003**, *107*, 6920−6931.
(34) He, G. S.; Lin, T.-C.; Cui, Y.; Prasad, P. N.; Brousmiche, D. W.; Serin, J. M.; Frechet, J. M. J. *Opt. Lett.* **2003**, *28*, 768−770.
(35) Brousmiche, D. W.; Serin, J. M.; Frechet, J. M. J.; He, G. S.; Lin, T.-C.; Chung, S. J.; Prasad, P. N. *J. Am. Chem. Soc.* **2003**, *125*, 1448−1449.
(36) Serin, J. M.; Brousmiche, D. W.; Frechet, J. M. J. *Chem. Commun.* **2002**, 2605−2607.
(37) Frechet, J. M. J. *Proc. Natl. Acad. Sci. U.S.A.* **2002**, *99*, 4782−4787.
(38) Das, P. K.; Encinas, M. V.; Scaiano, J. C. *J. Photochem.* **1980**, *12*, 357−361.
(39) Tamai, N.; Masuhara, H.; Mataga, N. *J. Phys. Chem.* **1983**, *87*, 4461−4467.
(40) Holden, D. A.; Guillet, J. E. *Macromolecules* **1980**, *13*, 289−295.
(41) Kamioka, K.; Webber, S. E. *Chem. Phys. Lett.* **1987**, *133*, 353−358.
(42) Fox, H. H.; Fox, M. A. *Macromolecules* **1995**, *28*, 4570−4576.
(43) Stewart, G. M.; Fox, M. A. *J. Am. Chem. Soc.* **1996**, *118*, 4354−4360.
(44) Kiserow, D. J.; Itoh, Y.; Webber, S. E. *Macromolecules* **1997**, *30*, 2934−2940.
(45) Ghaddar, T. H.; Whitesell, J. K.; Fox, M. A. *J. Phys. Chem. B* **2001**, *105*, 8729−8731.
(46) Würthner, F.; Thalacker, C.; Sautter, A. *Adv. Mater.* **1999**, *11*, 754−758.
(47) Würthner, F.; Sautter, A. *Chem. Commun.* **2000**, 445−446.
(48) Würthner, F.; Thalacker, C.; Sautter, A.; Schartl, W.; Ibach, W.; Hollricher, O. *Chem.—Eur. J.* **2000**, *6*, 3871−3886.
(49) Baudin, H. B.; Davidsson, J.; Serroni, S.; Juris, A.; Balzani, V.; Campagna, S.; Hammarström, L. *J. Phys. Chem. A* **2002**, *106*, 4312−4319.
(50) Balzani, V.; Campagna, S.; Denti, G.; Juris, A.; Serroni, S.; Venturi, M. *Acc. Chem. Res.* **1998**, *31*, 26−34.
(51) Denti, G.; Campagna, S.; Serroni, S.; Ciano, M.; Balzani, V. *J. Am. Chem. Soc.* **1992**, *114*, 2944−2950.
(52) Kirmaier, C.; Hindin, E.; Schwartz, J. K.; Sazanovich, I. V.; Diers, J. R.; Muthukumaran, K.; Taniguchi, M.; Bocian, D. F.; Lindsey, J. S.; Holten, D. *J. Phys. Chem. B* **2003**, *107*, 3443−3454.
(53) Zhao, Y.; Wasielewski, M. R. *Tetrahedron* **1999**, *40*, 7047−7050.
(54) van der Boom, T.; Hayes, R. T.; Zhao, Y.; Bushard, P. J.; Weiss, E. A.; Wasielewski, M. R. *J. Am. Chem. Soc.* **2002**, *124*, 9582−9590.
(55) van der Boom, T.; Evmenenko, G.; Dutta, P.; Wasielewski, M. R. *Chem. Mater.* **2003**, *15*, 4068−4074.
(56) Lukas, A. S.; Zhao, Y.; Miller, S. E.; Wasielewski, M. R. *J. Phys. Chem. B* **2002**, *106*, 1299−1306.
(57) Gosztola, D.; Niemczyk, M. P.; Svec, W.; Lukas, A. S.; Wasielewski, M. R. *J. Phys. Chem. A* **2000**, *104*, 6545−6551.
(58) Ego, C.; Marsitzky, D.; Becker, S.; Zhang, J.; Grimsdale, A. C.; Mullen, K.; MacKenzie, J. D.; Silva, C.; Friend, R. H. *J. Am. Chem. Soc.* **2003**, *125*, 437−443.

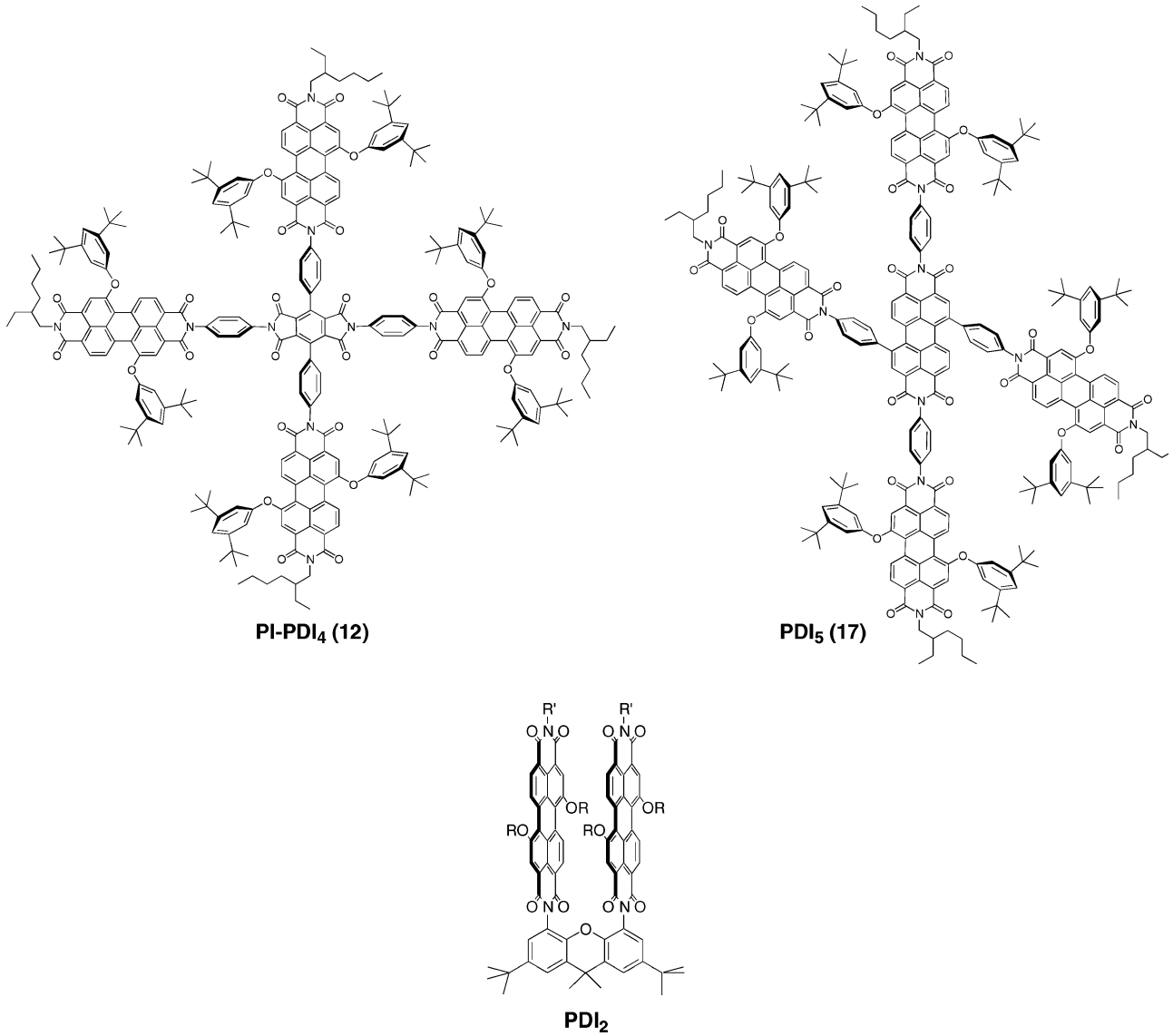

Figure 1. Structures of PI-PDI_4 and PDI_5 and reference molecule PDI_2, where R = 3,5-di-*tert*-butylphenyl and R′ = 2-ethylhexyl.

Experimental Section

General Information. The syntheses of PI-PDI_4 and PDI_5 as well as the intermediates leading to them are detailed in the Supporting Information. All solvents were spectrophotometric grade unless otherwise noted. Toluene was purified by passing it through series of CuO and alumina columns (GlassContour), while 2-methyltetrahydrofuran (Aldrich) was purified by passing it through a basic alumina column immediately prior to use. The sizes of the aggregates in solution were determined by gel permeation chromatography on a Hewlett-Packard 1100 HPLC system with a 4.6 × 300 mm^2 Waters Styragel HR-4E column. This column covers a molecular weight range from 50 to 100 000. The column was calibrated using polystyrene standards covering a molecular weight range of 2430−29 300. The sample diluent and mobile phase were 100% tetrahydrofuran (HPLC grade), and the standards and samples were passed through a 0.45 μm PTFE syringe filter prior to analysis. Both sample and standard solutions were prepared at a concentration of 0.1−0.2% (w/v). A 20 μL injection volume was used for both standard and sample solutions. An isocratic separation was performed with a run time of 25 min and a flow rate of 0.3 mL/min. The column temperature was controlled and kept at 40 °C, and the column output was monitored using a diode-array detector. Dynamic light scattering (DLS) experiments were performed with a Coulter N4 Plus instrument (632.8 nm light source). All solutions were filtered through a 0.45 μm PTFE filter prior to measurement, and care was taken to exclude any dust from the experimental setup. The angle of detection varied between 90° and 30°, and each sample was averaged using several hundred scans.

X-ray Scattering Measurements. X-ray scattering measurements were carried out using the undulator beam line 12-ID at the Advanced Photon Source (APS), Argonne National Laboratory. The X-ray scattering instrument utilized a double-crystal Si(111) monochromator and a two-dimensional mosaic CCD detector.[59] The X-ray wavelength was set at $\lambda = 1.0$ Å, and the sample to detector distances were adjusted to achieve scattering measured across two different q regions: 0.02 $Å^{-1} < q < 0.3$ $Å^{-1}$ and 0.1 $Å^{-1} < q < 1$ $Å^{-1}$, where $q = (4\pi/\lambda)\sin\theta$, λ is the X-ray wavelength, and 2θ is the scattering angle.

Solid Film Preparation and Characterization. Quartz plates (Chemglass) were cleaned by immersion in a freshly prepared "piranha" solution (concentrated H_2SO_4/H_2O_2 30% = 7:3 v/v) at 80 °C for at least 45 min. *Caution! This solution is an extremely strong oxidizing agent.* After cooling to room temperature, the slides were rinsed repeatedly with deionized (DI) water and subjected to an RCA-type cleaning procedure (H_2O/H_2O_2 30%/NH_4OH = 5:1:1 v/v/v), sonicating at room temperature for 45 min. The substrates were then rinsed with

(59) Seifert, S.; Winans, R. E.; Tiede, D. M.; Thiyagarajan, P. *J. Appl. Crystallogr.* **2000**, 782−784.

DI water and dried in an oven overnight at 115 °C. The freshly cleaned substrates were placed in an oven dried Schlenk-type reactor. A 50 mM solution of CH_3SiCl_3 in dry toluene solution was added and reacted for 5 h at 25 °C. The solution was then removed with a canulla. The functionalized substrates were washed twice with toluene, acetone, and methanol and dried under vacuum. Highly ordered pyrolytic graphite (HOPG) (SPI Supplies, SPI-2 grade) was freshly cleaved using Scotch tape immediately prior to use. A 10^{-4} M toluene solution of PDI_5 was either spun cast (Laurell WS-400) at 2000 rpm for 30 s or drop cast and dried at room temperature and stored in the dark under nitrogen until examination. The PDI_5 films were examined by tapping-mode atomic force microscopy using a Digital Instruments Multimode Nanoscope IIIa. The tips used were Nanoprobe TESP-70 with a cantilever length of 125 μm and a resonance frequency of 278−338 kHz. Optical absorption spectra of the film were recorded on the instrument described below.

Optical Spectroscopy. Steady-state absorption and emission spectra were performed on a Shimadzu 1601 UV/vis spectrophotometer and PTI single photon counting spectrofluorimeter in a right angle configuration, respectively. A 10 mm quartz cuvette was used for both the absorption and fluorescence measurements, and the optical density at λ_{max} for the fluorescence measurements was maintained at 0.1 ± 0.05 to avoid reabsorption artifacts.

Femtosecond transient absorption measurements were made using a regeneratively amplified titanium sapphire laser system operating at a 1 kHz repetition rate outfitted with a CCD array detector (Ocean Optics PC2000) for simultaneous collection of spectral and kinetic data.[60] The frequency-doubled output from the laser provides 400 nm, 80 fs pulses for excitation. Focusing a few microjoules of the 800 nm fundamental into a 1 mm sapphire disk generated a white light continuum probe pulse. All-reflective optics were used to focus the 800 nm pulse into the sapphire and recollimate the white light output, thus limiting the chirp on the white light pulse to < 200 fs from 450 to 800 nm. Cuvettes with a 2 mm path length were used, and the samples were irradiated with 0.5−1.0 μJ per pulse focused to a 200 μm spot. The optical density at λ_{max} was typically 0.4−0.8. The total instrument response function (IRF) for the pump−probe experiments was 130 fs. Kinetic analyses were performed at several wavelengths using a nonlinear least-squares fit to a general sum-of-exponentials using the Levenberg−Marquardt algorithm while accounting for the presence of the finite instrument response.

Fluorescence lifetime measurements were made using a Hamamatsu C4780 picosecond fluorescence lifetime measurement system, consisting of a C4334 Streakcope and a C4792-01 synchronous delay generator. The excitation light source was supplied by a home-built cavity-dumped Ti:Sapphire laser[61] with a NEOS N13389 3 mm fused-silica acousto-optic modulator (AOM). The AOM was driven by a NEOS Technologies N64389-SYN 10 W driver to deliver 38 nJ, sub-50 fs pulses at an 820 kHz repetition rate. The laser pulses were frequency doubled to 400 nm by focusing the 800 nm fundamental into a 1 mm Type I BBO crystal. The energy of the resulting blue pulses was attenuated to approximately 1.0 nJ/pulse for all fluorescence lifetime experiments. The total IRF of the streak camera system was 25 ps. The samples were prepared in glass cuvettes, and the optical density at the excitation wavelength was typically 0.020−0.035. At λ_{max} of the samples, the optical density was typically 0.080−0.105. All fluorescence data were acquired in single photon counting mode using the Hamamatsu HPD-TA software. The data were fit using the Hamamatsu fitting module and deconvoluted using the laser pulse profile. Two fits were generated for each experiment, one for the emission intensity integrated between 530 and 640 nm and another for the emission intensity integrated between 640 and 740 nm. Measurements were generally repeated 3 times, and the resulting time constants were averaged. Deviation from the mean was generally no worse than ±5%.

Results and Discussion

Synthesis. The synthesis of each multi-chromophoric array was carried out in two parts. First, a core molecule was synthesized; second, peripheral PDI chromophores were attached. This stepwise approach allows for the production of asymmetric systems that may prove useful in future studies of energy and/or electron transfer; see Figure 2. The first molecule contains a modified pyromellitimide (PI) core with four peripheral PDI chromophores held planar to one another to give $PI\text{-}PDI_4$. The PI core serves as a convenient 4-fold point of attachment and does not participate in either electron or energy transfer processes involving the attached PDI molecules. The second core molecule is itself a PDI modified at the 1 and 7 positions by the direct attachment of *p*-nitrophenyl groups. The 1,7-diphenyl-PDI core molecule is also surrounded by four PDI molecules to give PDI_5, in which all five PDI molecules lie in the same plane with respect to the core and each other in a rhombic structure. Substitution of 3,5-di-*tert*-butylphenoxy groups at the 1,7 positions of the peripheral PDI chromophores increases their solubility significantly. The ground-state absorption maxima of both 1,7-diphenyl and 1,7-diphenoxy substituted PDI derivatives shift from 520 nm in the parent molecule to 550 nm.[62]

The pyromellitimide core was prepared using a reaction sequence analogous to the known route to 3,6-diphenylpyromellitic dianhydride.[63] Treatment of durene with Br_2 and a catalytic amount of iodine in refluxing dichloromethane affords 1,4-dibromodurene, **1**, in 78% yield. Palladium-catalyzed cross coupling of 4-iodonitrobenzene and pinacolborane under basic conditions yielded nitroboronate ester **2** in 62% yield. This molecule is used directly in a Suzuki coupling with dibromodurene to give the dinitrotetramethylterphenyl **3** in 41% yield. Complete oxidation of the methyl groups of **3** to carboxylic acids is done in two stages using $KMnO_4$ in refluxing pyridine followed by $KMnO_4$ in refluxing aqueous NaOH to give **4** in 84% yield. The final dianhydride is obtained by treating **4** with glacial acetic acid and acetic anhydride at reflux temperature to give **5** in 37% yield. The second PDI core molecule is prepared by Stille coupling of 1,7-dibromoperylene-3,4:9,10-tetracarboxydianhydride[64] with *p*-(tri-*n*-butylstannyl)nitrobenzene in toluene catalyzed by $Pd(PPh_3)_4$ to give **13** in 66% yield.

The synthetic schemes used to attach the peripheral PDI derivatives to the core molecules differ slightly for each array because two different functionalized PDI derivatives are needed for the stepwise synthesis of $PI\text{-}PDI_4$, one with an anhydride, **8** to condense with the amine already present on the PI core, and one with an aniline group already incorporated into PDI, **9** to condense with the core dianhydride. In the case of PDI_5 only one type of functionalized PDI, **8**, is required. 1,7-Dibromoperylene-3,4:9,10-tetracarboxydianhydride is reacted with 3,5-di-*tert*-butylphenol in refluxing DMF in the presence of Cs_2CO_3 followed by precipitation of the product from glacial acetic acid

(60) Giaimo, J. M.; Gusev, A. V.; Wasielewski, M. R. *J. Am. Chem. Soc.* **2002**, *124*, 8530−8531.
(61) Pshenichnikov, M. S.; de Boerij, W. P.; Wiersma, D. A. *Opt. Lett.* **1994**, *19*, 572−575.
(62) Holtrup, F. O.; Muller, G. R. J.; Quante, H.; Feyter, S. D.; Schryver, F. C. D.; Müllen, K. *Chem.—Eur. J.* **1997**, *3*, 219−225.
(63) Schmitz, L.; Rehahn, M.; Balauff, M. *Polymer* **1993**, *34*, 646−649.
(64) Bohm, A.; Arms, H.; Henning, G.; Blaschka, P. BASF: German Patent No. DE 19547209A1, 1997.

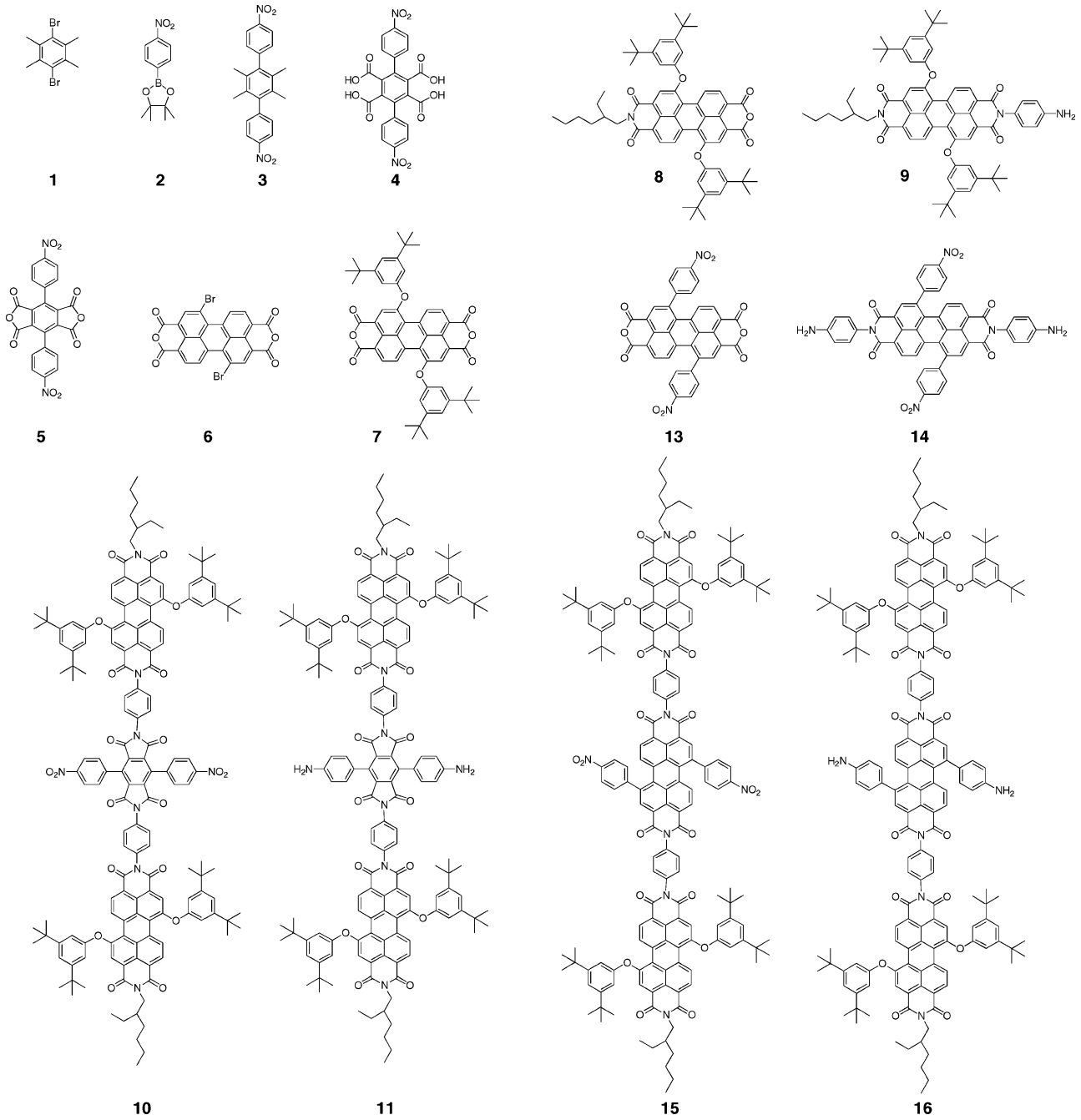

Figure 2. Structures of intermediates used to prepare PI-PDI$_4$ and PDI$_5$.

to give **7** in 90% yield. The dianhydride is converted to the monoanhydride-monoimide by reacting **7** with one molar equivalent of 2-ethylhexylamine in refluxing pyridine. Although a mixture of monoimide **8**, the diimide, and the dianhydride are obtained, the latter two can be separate easily and are recycled. Refluxing **8** in pyridine/imidazole with 1,4-diaminobenzene gives the target chromophore **9** in 83% yield. Reaction of dinitro compound **5** with amine **9** in the presence of imidazole in refluxing pyridine for 24 h produces **10** in 27% yield. Reduction of the nitro groups using $SnCl_2$ in THF under acidic conditions affords the diamine product **11** in quantitative yield. Finally, coupling of **11** with **8** in quinoline/zinc acetate at 180 °C for 4.5 days gives the target molecule PI-PDI$_4$, **12**, in 88% yield. Lower temperature solvents such as toluene, pyridine, and DMF did not produce the target compound, most likely because aggregation of the intermediate condensation product with three PDI molecules attached inhibits subsequent condensation of the fourth PDI to the core. Carrying out the condensation at higher temperatures reduces aggregation of the intermediate allowing better access of **8** to the amine leading to a higher yield of imide formation.

The synthesis of PDI$_5$ begins with the reaction of dinitrodianhydride **13** with 1,4-diaminobenzene in refluxing pyridine/imidazole for 6 h to give **14** in quantitative yield. Condensation of the first pair of PDI chromophores is performed by reacting **14** with excess anhydride **8** in pyridine/imidazole for 24 h to give **15** in 27% yield. Reduction of the nitro groups to the amines using $SnCl_2$ in THF under acidic conditions affords **16** in quantitative yield. Condensation of the remaining two PDI chromophores to complete the synthesis of PDI$_5$ is carried out

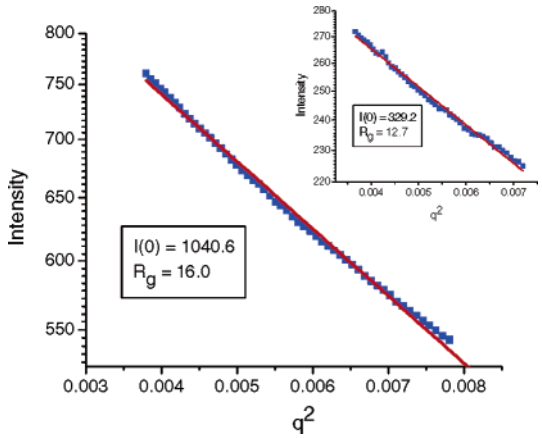

Figure 3. Guinier fit (solid line) of SAXS data for PDI5 in toluene. Inset: Guinier fit (solid line) for PDI_5 in THF.

by reacting **16** with an excess of **8** in quinoline/zinc acetate at 200 °C for 24 h to give **17** in 29% yield.

Characterization of Self-Assembled Structures. The mass spectrum of each chromophoric array was obtained using MALDI/TOF techniques. In addition to the parent ion (PI-PDI_4 = 4154 and PDI_5 = 4328) significant peaks are seen at several multiples of the molecular weight of each molecule. A distribution of aggregates with as many as 4 PI-PDI_4 and 13 PDI_5 molecules are readily seen in their mass spectra (Supporting Information, Figures S1A and S1B, respectively). These results are similar to that observed previously by us for ZnTPP−PDI_4.[20] Once again, these mass spectra give a strong indication of the tendency of the PDI molecule to self-assemble into larger structures. The ^{1}H NMR spectra of PI-PDI_4 and PDI_5 in deuterated chloroform, DMSO, toluene, and pyridine display severely broadened lines even at concentrations down to 10^{-5}M, which indicates that each of these molecules forms aggregates in these solvents. This is also the case for intermediates **15** and **16**. The observed broadening is illustrated for PDI_5 in chloroform in the Supporting Information, Figure S2.

To estimate the PDI_5 aggregate size we performed SAXS measurements on toluene and THF solutions using a high-flux synchrotron source (Advanced Photon Source (APS) at Argonne National Laboratory; see Experimental Section). The scattering intensity is a function of the scattering vector, q, which is related to the scattering angle 2θ by the relation $q = (4\pi/\lambda)\sin\theta$, where λ is the X-ray wavelength, Figure S3. We performed SAXS experiments in two different q regions: 0.02 Å^{-1} < q < 0.3 Å^{-1} and 0.1 Å^{-1} < q < 1 Å^{-1}, using two different sample-to-detector distances. In the low resolution scattering region below q = 0.1 Å^{-1}, the calculated scattering follows the Guinier relationship,[65−67] $I(q) = I(0)\exp(-q^2R_g^2/3)$, parametrized in terms of the forward scattering amplitude, $I(0)$, and the radius of gyration, R_g. Guinier plots of the PDI_5 data are presented in Figure 3. The linearity of Guinier plot is a measure of the monodispersity of the aggregate. The data for PDI_5 show essentially linear plots in both THF and toluene in the range 0.05 Å^{-1} < q < 0.09 Å^{-1} (0.003 Å^{-2} < q^2 < 0.008 Å^{-2}), indicating that the PDI_5 aggregates are monodisperse. In the q range below 0.05 Å^{-1} (below $q^2 \approx 0.003$ Å^{-2}) the experimental scattering data for PDI_5 in toluene and THF (note: this is more pronounced in THF) show concentration-dependent upward deviations from Guinier behavior that are characteristic of weakly associating molecular systems.[68] This can be linked to the propensity of PDI_5 to form large aggregates in the solid state as indicated by AFM measurements (see discussion below and Figure 7). The R_g is not directly related to the molecular structure but is the electron-density-contrast weighted sum of the squares of the atomic distances from the center of mass and, hence, depends on a combination of factors including electron density contrast with the solvent and structure of the solvent-excluded and solvent-associated layers.[66,67] Thus, for PDI_5 in toluene R_g = 16.0 ± 0.1 Å, and in THF R_g = 12.7 ± 0.1 Å. The variation in R_g values in two solvents may indicate somewhat dissimilar structures and/or different solvent−solute interactions in toluene vs THF. It should be noted that R_g values for PDI_5 indicate that it forms small aggregates in toluene and THF solution.

The Guinier plot also yields the extrapolated intensity at zero scattering angle, $I(0)$, which can be used to estimate the molecular weight of the aggregate by comparison to an $I(0)$ value of a reference compound of similar structure with known molecular weight (provided both compounds demonstrate linear Guinier plots).[67] Our reference of choice was a π-stacked dimer of a 3-fold symmetric tris(PDI) derivative, Figure S4A, which demonstrates excellent SAXS characteristics (Figures S4B and S4C), while its dimeric structure was independently established by a variety of methods (see Supporting Information). The estimated molecular weight of PDI_5 is ∼7600 in toluene and ∼7800 in THF, indicating that PDI_5 forms dimers in these solvents.

We used gel permeation chromatography (GPC) to independently determine the sizes of the PI-PDI_4 and PDI_5 aggregates in solution at approximately 10^{-5} M, the concentration at which the optical experiments reported here are performed. The GPC data, Supporting Information Figure S5, show that the aggregates of both PI-PDI_4 and PDI_5 are dimers with a polydispersity of 1.1, which agrees very well with the SAXS data for PDI_5. Dynamic light scattering experiments using a 632.8 nm laser source (Coulter N4 Plus) on solutions of PI-PDI_4 and PDI_5 at concentrations as high as 10^{-3} M in toluene show only very weak scattering signals, which indicates that, even at this higher concentration, the aggregate sizes remain at or below the ∼3 nm size measurement limit of the light scattering instrument.

The optical absorption spectra of PI-PDI_4 and PDI_5 in toluene, 2-methyltetrahydrofuran (MTHF), and chloroform shown in Figures 4 and 5, respectively, provide evidence for the orientation of the transition moment axes of the PDI chromophores[69] relative to one another within the aggregates. The lowest energy absorption band of the PDI monomer is found at 550 nm,[20] while, in the case of $(PI\text{-}PDI_4)_2$, there are two bands at 510 and 545 nm and, for $(PDI_5)_2$, these bands are at 515 and 550 nm. Very similar spectra were observed for the fully covalent dimeric PDI_2 reference molecule, Figure 1,[20] in which the transition dipoles for the lowest energy transitions in each of the two PDI chromophores, which lie along their N−N axes, are constrained

(65) Guinier, A.; Fournet, G. *Small Angle Scattering*; Wiley: New York, 1955.
(66) Glatter, O. In *Neutron, X-ray and Light Scattering*; Lindner, P., Zemb, T., Eds.; Elsevier: Amsterdam, 1991; pp 33−82.
(67) Glatter, O.; Kratky, O. *Small-Angle X-ray Scattering*; Academic Press: London, 1982.
(68) Ducruix, A.; Guilloteau, J. P.; Ries-Kautt, M.; Tardieu, A. *J. Cryst. Growth* **1986**, *168*, 28−39.
(69) Fritz, K. P.; Scholes, G. D. *J. Phys. Chem. B* **2003**, *107*, 10141−10147.

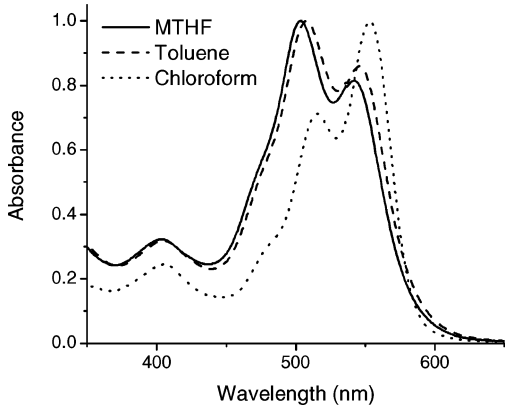

Figure 4. Normalized optical absorption spectra PI-PDI_4.

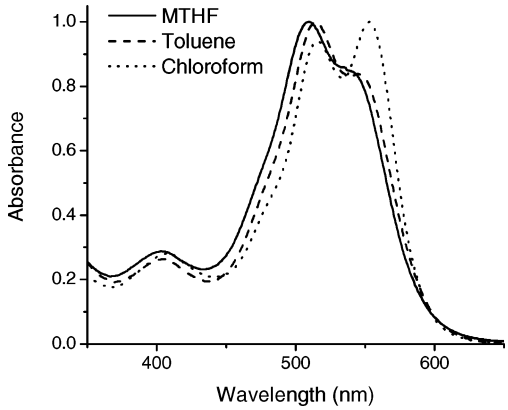

Figure 5. Normalized optical absorption spectra of PDI_5.

to a parallel orientation. If the transition dipoles of two identical chromophores are positioned in a parallel, stacked geometry, the molecular exciton model predicts that coupling of the two transition dipoles will cause the lowest energy electronic transition of the dimer to split into two bands with the higher-energy band having all of the oscillator strength.[70] The presence of the intense 510 and 515 nm bands in $(PI\text{-}PDI_4)_2$ and $(PDI_5)_2$ suggests that the PDI molecules in these assemblies adopt a parallel, stacked geometry. However, the spectra do not preclude the possibility that any two PDI molecules within the stacks may deviate somewhat from a strictly cofacial orientation relative to one another to minimize steric interactions. For example, sideways slippage of parallel aromatic planes either along the N−N axis of PDI (*y*-axis) or along the in-plane axis perpendicular to it (*x*-axis) may occur. In addition, a small degree of tipping of the aromatic planes may occur. Small slippage of the planes along the *x*-axis will not alter the spectrum greatly because the transition moments of the two PDI molecules remain parallel to one another. Slippage of one PDI molecule relative to another along the *y*-axis, as measured by the angle between a vector normal to the aromatic planes (*z*-axis) and a vector joining the centers of the two PDI molecules must be considerably less than 54.7° (the magic angle) in order to preserve the dominance of the blue-shifted absorbance.[70] Finally, significant tipping of the aromatic planes relative to one another along the *z*-axis will result in a rapid decrease in exciton coupling due to the $1/r^3$ dependence of this interaction.

The optical transition from the ground state of $(PI\text{-}PDI_4)_2$ and $(PDI_5)_2$ to their lower exciton states, which is symmetry forbidden in the molecular exciton model for H-aggregates, still has significant oscillator strength as evidenced by the intensity of the band at 550 nm. Extension of the simple molecular exciton model to include vibronic coupling in the exciton states of the dimer relieves the symmetry restrictions inherent to the simple model.[71,72] Thus, the 510 nm band is the transition from the ground state to the $\upsilon = 0$ vibronic level of the upper exciton state, while the 550 nm band is the corresponding transition to the $\upsilon = 1$ vibronic level of the lower exciton state. The greater oscillator strength of the 510 nm transition in PDI is consistent with the geometry of face-to-face stacking. The presence of the low energy transition is evident in the spectra of both $(PI\text{-}PDI_4)_2$ and $(PDI_5)_2$. This behavior is also observed in the solvent-independent spectra of PDI_2 in which the orientation of the two PDI molecules relative to one another is constrained to a parallel, cofacial geometry by the xanthene spacer.[20] Nevertheless, it is also possible that a small fraction of the residual 550 nm absorption in the spectra of both $(PI\text{-}PDI_4)_2$ and $(PDI_5)_2$ is due to residual monomeric PDI molecules in equilibrium with the aggregates.

For PDI_5, we see a strong tendency to aggregate in toluene and MTHF, and to a lesser degree in chloroform. Aggregation is driven by strong $\pi-\pi$ interactions between adjacent PDI chromophores. For example, intermediate **15**, which contains three PDI chromophores in a linear array, also exhibits an intense blue-shifted band at 510 nm (Supporting Information, Figure S6). Given that the intramolecular chromophores are in an end-to-end arrangement, the coplanar orientation of the PDI π systems makes it possible for the PDI molecules to form parallel stacked aggregates as indicated by the appearance of the 510 nm absorption feature. In the case of $PI\text{-}PDI_4$, the same general trends are observed; aggregate formation is more significant in toluene and MTHF and less so in chloroform.

Two of the simplest possible stacking motifs for $(PI\text{-}PDI_4)_2$ and $(PDI_5)_2$ are illustrated in Figure 6A and B, respectively. These structures were calculated using the MM+ force field.[73] The $PI\text{-}PDI_4$ dimer structure in Figure 6A is rather flat, while two saddle-shaped PDI_5 molecules nest to form the PDI_5 dimer shown in Figure 6B. The average distance between the stacked PDI molecules in $(PI\text{-}PDI_4)_2$, as well as between the stacked peripheral PDI molecules in $(PDI_5)_2$, is 3.5 Å. The distance between the central PDI molecules in $(PDI_5)_2$ is 5.1 Å. Although these structures are not unique due to rotational isomers about the single bonds joining the peripheral PDI molecules to the core, the optical spectra require that each PDI chromophore is stacked on a partner PDI chromophore with their transition moments parallel.

The sizes and structures of aggregates in solution frequently differ greatly from those deposited as films. We have used scanning probe microscopy techniques[74−76] to examine the

(70) Kasha, M.; Rawls, H. R.; El-Bayoumi, M. A. *Pure Appl. Chem.* **1965**, *11*, 371−392.
(71) Fulton, R. L.; Gouterman, M. *J. Chem. Phys.* **1964**, *41*, 2280−2286.
(72) Oddos-Marcel, L.; Madeore, F.; Bock, A.; Neher, D.; Ferencz, A.; Rengel, H.; Wegner, G.; Kryschi, C.; Trommsdorff, H. P. *J. Phys. Chem.* **1996**, *100*, 11850−11856.
(73) MM+ calculations were performed using HyperChem(TM), Hypercube, Inc., 1115 NW 1114th Street, Gainesville, FL 32601, USA.
(74) Jonkheijm, P.; Miura, A.; Zdanowska, M.; Hoeben, F.; Feyter, S.; Schenning, A.; Schryver, F.; Meijer, E. *Angew. Chem., Int. Ed.* **2004**, *43*, 74−78.
(75) Liu, D. F. S.; Grim, P.; Vosch, T.; Grebel-Koehler, D.; Wiesler, U.; Berresheim, A.; Muellen, K. Schryver, F. *Langmuir* **2002**, *18*, 8223−8230.

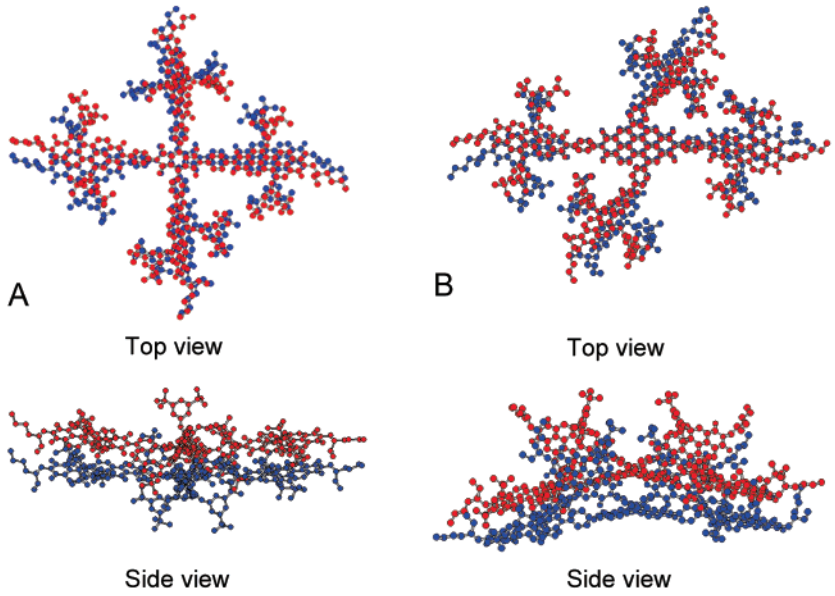

Figure 6. MM+ calculated structures of (A) $(PDI_5)_2$ and (B) $(PI\text{-}PDI_4)_2$. Views are along the stacking direction (top) and an axis 90° to that direction (side).

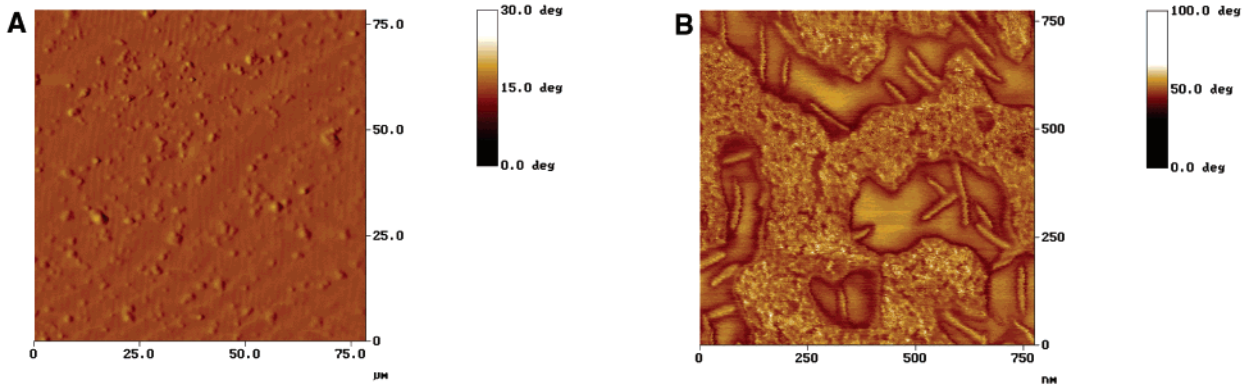

Figure 7. AFM phase contrast images of PDI_5. (A) PDI_5 spin-cast from toluene onto methylated quartz; (B) PDI_5 drop-cast from toluene onto HOPG.

nature of $(PDI_5)_n$ in the solid state. To this end, thin solid films of $(PDI_5)_n$ were prepared on both methylsilylated quartz[55] and freshly cleaved highly ordered pyrolytic graphite (HOPG) substrates and examined using atomic force microscopy (AFM). Blank slides of both substrates were used to verify the smoothness and morphology of each substrate. Spin-cast films of PDI_5 prepared using quartz slides produced columnar structures with a broad distribution of sizes having an average height of 138 ± 94 nm and an average width of 2.09 ± 0.89 μm, Figure 7A. No columnar structures were observed on nonmethylsilylated quartz slides, where substantial dewetting of the films on the hydrophilic quartz surfaces occurred. Drop-cast films made on HOPG, Figure 7B, reveal that PDI_5 is substantially more ordered than observed for films on methylsilylated quartz. The film appears to consist of packed rod-shaped nanostructures. When the rods are packed perpendicular to the surface, they form a 19 ± 4 nm thick layer. The rods that have grown in directions parallel to the surface are generally much longer, exhibiting dimensions that average (11 ± 3) × (45 ± 10) × (131 ± 28) nm^3. The growth of these structures in the direction perpendicular to the surface is limited relative to the lengths they can attain when they grow parallel to the surface. As is usually the case, the solid-state morphology of these films is affected by surface hydrophobicity, substrate roughness, sample concentration, solvent choice, and method of thin-film growth. Spin-cast films on methylsilylated quartz exhibit ground-state absorption spectra that are similar to those observed in solution (Supporting Information Figure S7). The similarity between the spectra of the aggregates in solution and on the methylsilylated quartz films suggests that the H-aggregation motif observed in solution is also preserved to a large degree in the films. The optical absorption spectra of the HOPG based films could not be obtained due to the opaque nature of the substrate.

Photophysics of Self-Assembled Structures. Steady-state fluorescence measurements were performed on solutions of $PI\text{-}PDI_4$ and PDI_5 in toluene, MTHF, and chloroform. Each sample was excited at 500 nm, and rhodamine 640 served as the standard for measuring emission quantum yields. This standard was chosen for its well-characterized emission from 550 to 750 nm, which is nearly identical to the wavelength range of the PDI emission in these molecules. As seen in Figure 8, the emission of $(PI\text{-}PDI_4)_2$ in all three solvents is red-shifted compared to the PDI monomer. In MTHF and toluene, this band is broadened relative to the PDI monomer. A new red-shifted emission band appears in both toluene and MTHF, while the

(76) Schenning, A.; Herrikhuyzen, J.; Jonkheijm, P.; Chen, Z.; Würthner, F.; Meijer, E. *J. Am. Chem. Soc.* **2002**, *124*, 10252−10253.

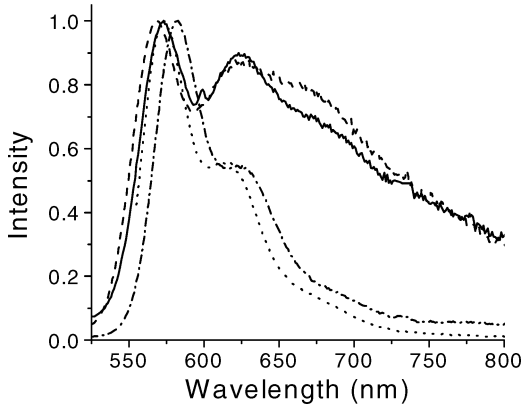

Figure 8. Normalized fluorescence spectra of PI-PDI$_4$ in toluene (—), MTHF (- - -), and $CHCl_3$ (-•-•-) compared to that of PDI in $CHCl_3$ (••••).

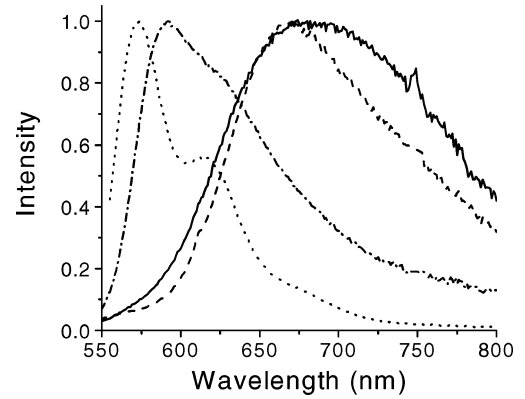

Figure 9. Normalized fluorescence spectra of PDI$_5$ in toluene (—), MTHF (- - -), and $CHCl_3$ (-•-•-) compared to that of PDI in $CHCl_3$ (••••).

Table 1. Fluorescence Quantum Yields

	toluene		MTHF		chloroform	
compound	530–640 nm	640–825 nm	530–640 nm	640–825 nm	530–640 nm	640–825 nm
PI-PDI$_4$	0.12	0.15	0.07	0.08	0.40	0.16
PDI$_5$	0.04	0.19	0.02	0.13	0.15	0.12
PDI$_2$[a]		0.15		0.13		0.06
PDI[b]	0.96		0.98		0.86	

[a] PDI$_2$ exhibits a single fluorescence emission band with $\lambda_{max} = 700-720$ nm. [b] PDI exhibits a single fluorescence emission band with $\lambda_{max} = 550$ nm.

emission feature in chloroform is very similar to that of monomeric PDI. This effect is even more pronounced for $(PDI_5)_2$, Figure 9. The red-shifted emission of $(PDI_5)_2$ dominates in both toluene and MTHF, and is even apparent to some degree in chloroform. The changes in the emission spectra of PI-PDI$_4$ and PDI$_5$ as a function of solvent track the observed changes in the ground state absorption spectra, where aggregate formation in chloroform is significantly reduced relative to that in both toluene and MTHF. The fluorescence quantum yields given in Table 1 also support this trend, where the highest fluorescence quantum yields are observed in chloroform.

The large Stokes shift and the width of the new broad emission feature that appears in Figures 8 and 9 relative to that of monomeric PDI suggest that this transition is due to formation of an excimer-like state. A strongly red-shifted emission has been observed previously in covalent dimers of PDI[77] including

(77) Langhals, H.; Ismael, R. *Eur. J. Org. Chem.* **1998**, 1915−1917.

Table 2. Fluorescence Lifetime Data

		530–640 nm				640–740 nm			
compd	solvent	τ_1 (ns)	A_1	τ_2 (ns)	A_2	τ_1 (ns)	A_1	τ_2 (ns)	A_2
PI-PDI$_4$	chloroform	4.54	1.00			4.53	1.00		
PI-PDI$_4$	MTHF	4.40	0.98	17.9	0.02	4.35	0.77	18.9	0.23
PI-PDI$_4$	toluene	4.32	0.98	21.4	0.02	4.12	0.78	21.7	0.22
PDI$_5$	chloroform	5.58				6.15			
PDI$_5$	MTHF	4.59	0.96	14.8	0.04	4.78	0.65	15.9	0.35
PDI$_5$	toluene	4.42	0.94	17.6	0.06	4.67	0.63	20.3	0.37
PDI$_2$[a]	chloroform					14.6	1.0		
PDI$_2$[a]	MTHF					19.7	1.0		
PDI$_2$[a]	toluene					22.8	1.0		

[a] All fluorescence decays of PDI$_2$ are monoexponential.

PDI$_2$ (see below). Thus, even though the PDI molecules are associated in the ground state, and thus the state is not a true excimer, the interaction between the PDI chromophores becomes stronger in the excited state.[78−80] The measured quantum yields of emission from this band are significant, Table 1. For example, the quantum yields of excimer-like emission for $(PI\text{-}PDI_4)_2$ and $(PDI_5)_2$ in toluene are 0.15 and 0.19, respectively, and are similar to that observed for PDI$_2$.

Time-resolved fluorescence spectroscopy on PI-PDI$_4$ and PDI$_5$ was carried out in toluene, MTHF, and chloroform, Table 2. The excitation intensity was kept low (1 nJ/pulse) to avoid exciton annihilation processes (see below). Time constants down to about 5 ps can be obtained by deconvolution of the IRF from the data. The fluorescence lifetime data for both $(PI\text{-}PDI_4)_2$ and $(PDI_5)_2$ reveal biexponential decays in both toluene and MTHF and single exponential decays in chloroform. In the 530−640 nm wavelength range, the fluorescence lifetimes of $(PI\text{-}PDI_4)_2$ and $(PDI_5)_2$ in all solvents are dominated by a 4−5 ns component, which is very similar to that observed for monomeric PDI in these solvents. However, in the 640−740 nm wavelength range, a significant fraction of the total amplitude corresponds to a much longer emission component, which varies from 17 to 22 ns. The amplitude of this long component does not dominate the decay because the radiative rate of the long wavelength emitting species is smaller than that of the residual PDI monomers. This results in contamination of the long wavelength emission band by the tail of the PDI monomer emission. It is interesting to note that our observed lifetime for the long wavelength emission at 640−740 nm is very similar to the 17 ns lifetime observed for perylene excimers by Katoh et al..[79] Moreover, our own results show that in PDI$_2$ the excimer-like emission dominates completely and exhibits monoexponential fluorescence lifetimes that are long (15−23 ns), Table 2. Since the absorption spectrum of PDI$_2$ is only weakly dependent on solvent, the small variation in PDI$_2$ fluorescence lifetime and fluorescence quantum yield is most likely due to small changes in radiative rate and perhaps a heavy atom effect in $CHCl_3$.

Femtosecond photoexcitation of $(PI\text{-}PDI_4)_2$ and $(PDI_5)_2$ in toluene with either 400 or 550 nm laser pulses yields similar transient absorption spectra. Typical spectra for $(PDI_5)_2$ are shown in Figure 10, while that of $(PI\text{-}PDI_4)_2$ is shown in the Supporting Information, Figure S8. The ground-state absorption

(78) Michl, J.; Bonacic-Koutecky, V. *Electronic Aspects of Organic Photochemistry*; John Wiley and Sons: New York, 1990; pp 274−385.
(79) Katoh, R.; Sinha, S.; Murata, S.; Tachiya, M. *J. Photochem Photobiol., A* **2001**, *145*, 23−34.
(80) Stevens, B. In *Advances in Photochemistry*; Pitts, J. N., Hammond, G. S., Noyes, W. A., Eds.; Wiley-Interscience: 1971; Vol. 8, pp 194−198.

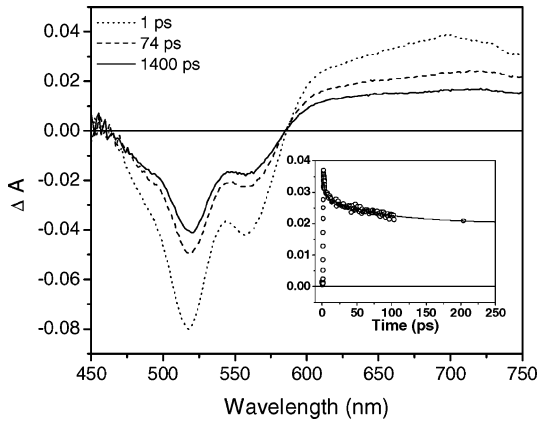

Figure 10. Transient absorption spectra of $(PDI_5)_2$ in toluene following excitation at 400 nm. Inset: kinetics at 715 nm.

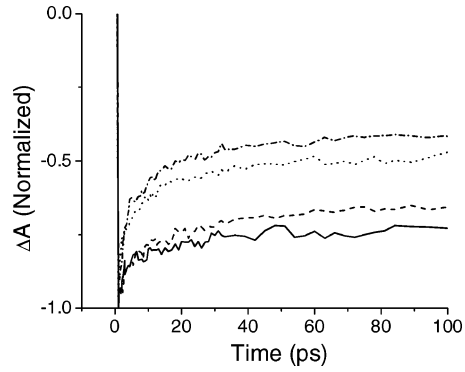

Figure 11. Transient absorption kinetics for $(PDI_5)_2$ in toluene monitored at 520 nm following excitation with 400 nm, 80 fs laser pulses having 0.25 (—), 0.5 (- - -), 2.0 (•••••), and 2.5 (-•-•-) μJ per pulse focused to a 200 μm diameter spot size.

spectrum bleaches immediately upon excitation and is accompanied by a broad excited-state absorption that extends from 580 nm to past 750 nm. The broad, ill-defined nature of the 580−750 nm absorption is similar to that observed for PDI within PDI_2[20] and is indicative of a strong interaction between the excited PDI molecule and its neighboring PDI. The inset shows the transient absorption kinetics of this band at 715 nm. The transient absorption kinetics for the recovery of the ground-state bleach at 510 nm (not shown) match those for the decay of the excited state at 715 nm. The appearance kinetics for these features is IRF limited, and the decay kinetics display two components for $(PI\text{-}PDI_4)_2$, $\tau = 19$ ps and >3 ns, as well as for $(PDI_5)_2$, $\tau = 17$ ps and >3 ns. The transient spectra and kinetics are independent of whether 400 or 550 nm excitation is used, so that the fast component is not due to relaxation of an upper excited state, such as the upper exciton state.

In both $(PI\text{-}PDI_4)_2$ and $(PDI_5)_2$, a significant fraction of the excited-state population decays to the ground state with $\tau = 19$ and 17 ps, respectively. The spectra of the ground-state bleaches do not evolve in time, indicating that the ground-state product of the photoinduced event is the same as the initial state, i.e., the PDI chromophores remain aggregated throughout the excited-state decay process. It is well-known that ultrafast laser excitation of dye aggregates including photosynthetic antenna proteins having large absorption cross sections often leads to multiple excitations of the chromophore array resulting in exciton annihilation processes.[81−85] To probe whether the rapid initial transient absorption changes observed for $(PI\text{-}PDI_4)_2$ and $(PDI_5)_2$ are due to this process, transient absorption kinetics as a function of the laser pump pulse energy were measured with 400 nm excitation, which are illustrated for $(PDI_5)_2$ in Figure 11. The kinetics at 520 nm, normalized at the maximum ΔA, clearly show that the fraction of molecules that undergo fast deactivation increases as the pulse energy increases, which is typical of singlet−singlet exciton annihilation.

Laser excitation of large arrays of chromophores frequently results in the formation of several excited chromophores within the array.[86] Dependent on the size of the chromophore array and the degree of electronic interaction between the chromophores, migration of the singlet excitons within the array leads to singlet−singlet exciton annihilation as an important decay pathway for the excitons. When two excitons collide, they can form a variety of products,[85,87,88] the most typical being an upper excited singlet state and a ground singlet state.[81,89] The upper excited singlet state quickly relaxes back to the lowest excited singlet state, so the net effect is the loss of one exciton. These dynamics exhibit classic "predator-prey" type behavior; i.e., the more excitons that are available, the more annihilations occur.[89] However, this quickly depletes the number of excitons available, so fewer annihilations can occur. Increased pump power creates more excitons and, thus, more annihilation events, leading to an increase in the ΔA for this process.[81,84] It is important to note that the conditions for annihilation, multiple excitons in an array, generally only occur when very high intensity laser pulses are employed. This behavior is usually not seen in conventional steady-state measurements at low photon fluxes, where it would manifest itself as a decrease in fluorescence quantum yield.

Singlet−singlet annihilation is a second-order kinetic process, so that the simplest description of excited singlet state decay in the presence of annihilation is given by eq 1:[87,90]

$$-\frac{d\Delta A}{dt} = \gamma_1 \Delta A + \frac{1}{2}\gamma_2 (\Delta A)^2 \qquad (1)$$

where γ_1 is the overall rate constant for unimolecular decay of the excited singlet state and γ_2 is the time independent rate constant for singlet−singlet annihilation defined as the annihilation rate per pair of excitons in a domain and has the dimensions of s^{-1}.[84,91,92] The annihilation rate constant γ_2 depends critically on the number of electronically connected chromophores in the aggregate (the domain size), as well as the strength of the

(81) Bittner, T.; Irrgang, K.-D.; Renger, G.; Wasielewski, M. R. *J. Phys. Chem.* **1994**, *98*, 11821−11826.
(82) Bittner, T.; Viogt, J.; Irrgang, K.-D.; Renger, G. *Photochem. Photobiol.* **1993**, *57*, 158−162.
(83) van Grondelle, R. *Biochim. Biophys. Acta* **1985**, *811*, 147−195.
(84) Gillbro, T.; Sandstrom, A.; Spanfort, M.; Sundstrom, V.; van Grondelle, R. *Biochim. Biophys. Acta* **1988**, *934*, 369−374.
(85) Geacintov, N. E.; Breton, J. In *Biological Events Probed by Ultrafast Laser Spectroscopy*; Alfano, R. R., Ed.; Academic Press: New York, 1982; pp 158−191.
(86) Den Hollander, W. T. F.; Bakker, J. G. C.; van Grondelle, R. *Biochim. Biophys. Acta* **1988**, *725*, 492−507.
(87) Swenberg, C. E.; Geacintov, N. E. *Org. Mol. Photophys.* **1973**, *18*, 489−565.
(88) Khairutdinov, R. F.; Serpone, N. *J. Phys. Chem. B* **1997**, *101*, 2602−2610.
(89) Pope, M.; Swenberg, C. E. *Electronic Processes in Organic Crystals and Polymers*, 2nd ed.; Oxford University Press: New York, 1999; Vol. 56, pp 157−161.
(90) Paillotin, G.; Swenberg, C. E.; Breton, J.; Geacintov, N. E. *Biophys. J.* **1979**, *25*, 513−534.
(91) Paillotin, G.; Swenberg, C. E.; Breton, J.; Geacintov, N. E. *Biophys. J.* **1979**, *25*, 513−534.
(92) Barzda, V.; Gulbinas, V.; Kananavicius, R.; Cervinskas, V.; van Amerongen, H.; van Grondelle, R.; Valkunas, L. *Biophys. J.* **2001**, *80*, 2409−2421.

coupling. For example, studies on the LH2 antenna protein from the purple bacterium *Rhodospirillum rubrum* found an annihilation rate constant, τ_a, of 1×10^{12} s^{-1} for a domain of 30 chromophores.[93] More recent studies on this system used a domain size of 12 and found a rate of 2×10^{12} s^{-1}.[94] Workers studying the Fenna−Matthews−Olsen antenna protein from the green sulfur bacterium *Chlorobium tepidum* found a rate of 1.4×10^{11} s^{-1} for a domain of 21 units.[95] Bittner et al.[81] have shown that τ_a for the trimeric LHCII light-harvesting protein from photosystem II of green plants, which contains 21 chlorophyll *a* molecules, is 25 ps, which was corroborated by the more recent study of Bardza et al..[92] For both $(PI\text{-}PDI_4)_2$ and $(PDI_5)_2$ in which the exciton can migrate between a small number of sites, the observed time constant for the annihilation process, τ_a, can be related to the site-to-site hopping time constant, τ_{hop}, using eq 2:[96]

$$\tau_a = 2\gamma_2^{-1} = (\pi^{-1}N \ln N + 0.20N - 0.12)\tau_{hop} \qquad (2)$$

where N is the number of sites. Equation 2 assumes that every collision of two excitons results in rapid annihilation, so that τ_a is limited by the exciton hopping rate τ_{hop}, not by the trapping rate. In addition, eq 2 assumes the exciton hops between nearest neighbor sites on a square lattice with equal probability. Since the excimer-like state in both $(PDI_4{-}PI)_2$ and $(PDI_5)_2$ forms within the 130 fs instrument response function of the experiment, we will assume that the migrating exciton is initially delocalized between two adjacent π-stacked PDI molecules within each dimer. In that case, the exciton hops between four sites within $(PDI_4{-}PI)_2$ and five sites within $(PDI_5)_2$. Substituting $N = 4$ and 5 and the 19 and 17 ps annihilation time constants for $(PDI_4{-}PI)_2$ and $(PDI_5)_2$, respectively, into eq 2 yields $\tau_{hop} = 7.8$ ps and $\tau_{hop} = 4.9$ ps for $(PDI_4{-}PI)_2$ and $(PDI_5)_2$, respectively. These hopping times are very similar to those estimated for the trimeric LHC-II photosynthetic light harvesting antenna complex containing 21 chromophores, where typically $\tau_{hop} \cong 4{-}5$ ps (for a recent summary, see ref 92). It is most likely that the value of τ_{hop} differs for exciton hops between sites that are covalently bonded versus those that are not. Moreover, different covalent connections between the PDI molecules will also result in different values of τ_{hop}. In the work presented here our experimental data cannot distinguish between these routes. In future studies we will explore specific structures designed to differentiate between these pathways.

Conclusions

Two different multi-chromophoric arrays $PI\text{-}PDI_4$ and PDI_5 based on the PDI chromophore were synthesized and characterized. These arrays self-assemble into partially ordered supramolecular dimers $(PI\text{-}PDI_4)_2$ and $(PDI_5)_2$ in solution as indicated by both SAXS and GPC data, where the PDI molecules are approximately parallel and cofacial to one another. Photoexcitation of these supramolecular dimers gives direct evidence of strong $\pi{-}\pi$ interactions between the excited PDI chromophore and other PDI molecules nearby based on the observed formation of an excimer-like state in <130 fs with a lifetime of about 20 ns. Multiple photoexcitation of these supramolecular dimers leads to fast singlet−singlet annihilation of the excimer-like states, which indicates that the electronic interaction among the chromophores is strong. While singlet−singlet annihilation is well-known in J-aggregates,[88,97,98] relatively few studies have demonstrated singlet−singlet annihilation in H-aggregates due to the forbidden nature of the direct transition to ground state.[88,99] The population of the nearby excimer-like state in $(PI\text{-}PDI_4)_2$ and $(PDI_5)_2$, followed by its allowed radiative transition to the ground state, makes the annihilation events observable. Atomic force microscopy reveals that solutions of $(PDI_5)_2$ assemble into large rod-shaped nanostructures with an average length 130 nm on flat substrates. The supramolecular PDI antenna structures presented here are promising as efficient energy transport materials, a quality that is highly desirable in both solar cell and light-emitting diode applications.

Acknowledgment. This paper is dedicated to Professor Frederick D. Lewis on the occasion of his 60th birthday. This work was supported by the National Science Foundation (CHE-0102351) and the Office of Naval Research (N00014-02-1-0381). Work at the Argonne National Laboratory was supported by the Division of Chemical Sciences, Office of Basic Energy Sciences, U.S. Department of Energy under Contract W-31-109-Eng-38. The authors wish to thank Emily Weiss for many helpful discussions, Prof. P. Messersmith for the use of his DLS apparatus, and Ms. Jennifer Bash for carrying out the GPC studies.

Supporting Information Available: Details regarding the synthesis and characterization of the molecules used in this study. This material is available free of charge via the Internet at http://pubs.acs.org.

JA039820C

(93) Deinum, G.; Aartsma, T. J.; van Grondelle, R.; Amesz, J. *Biochim. Biophys. Acta* **1989**, *976*, 63−69.
(94) Valkunas, L.; Trinkunas, G.; Liuolia, V.; van Grondelle, R. *Biophys. J.* **1995**, *69*, 1117−1129.
(95) Gulbinas, V.; Valkunas, L.; Kuciauskas, D.; Katilius, E.; Liuolia, V.; Zhou, W.; Blankenship, R. E. *J. Phys. Chem.* **1996**, *100*, 17950−17956.
(96) Montroll, E. W. *J. Math. Phys.* **1969**, *10*, 753−765.
(97) Ozcelik, S.; Akins, D. L. *J. Phys. Chem. B* **1997**, *101*, 3021−3021.
(98) Holzer, W.; Penzkofer, A.; Stockman, R.; Meysel, H.; Liebegott, H.; Horhold, H. H. *Synth. Met.* **2002**, *125*, 343−357.
(99) Ern, J.; Bock, A.; Oddos-Marcel, L.; Rengel, H.; Wegner, G.; Trommsdorff, H. P.; Kryschi, C. *J. Phys. Chem. A* **1999**, *103*, 2446−2450.